

# 1 Characterizing Long-term Wear and Tear of 2 Ion-Selective pH Sensors

3 Kito Ohmura<sup>a,b</sup>, Christian M. Thürlimann<sup>a,c</sup>, Marco Kipf<sup>a</sup>, Juan Pablo  
4 Carbajal<sup>a</sup>, Kris Villez<sup>a,c,\*</sup>

5 <sup>a</sup>*Eawag, Überlandstrasse 133, CH-8600 Dübendorf, Switzerland*

6 <sup>b</sup>*Toshiba Infrastructure Systems & Solutions Corporation, Tokyo, Japan*

7 <sup>c</sup>*ETH Zürich, Institute of Environmental Engineering, 8093 Zürich, Switzerland*

---

## 8 Abstract

The development and validation of methods for fault detection and identification in wastewater treatment research today relies on two important assumptions: *(i)* that sensor faults appear at distinct times in different sensors and *(ii)* that any given sensor will function near-perfectly for a significant amount of time following installation. In this work, we show that such assumptions are unrealistic, at least for sensors built around an ion-selective measurement principle. Indeed, long-term exposure of sensors to treated wastewater shows that sensors exhibit important fault symptoms that appear simultaneously and with similar intensity. Consequently, our work suggests that focus of research on methods for fault detection and identification should be reoriented towards methods that do not rely on the assumptions mentioned above. This study also provides the very first empirically validated sensor fault model for wastewater treatment simulation and we recommend its use for effective benchmarking of both fault detection and identification

---

\*Corresponding author, Email [kris.villez@eawag.ch](mailto:kris.villez@eawag.ch)

methods and advanced control strategies. Finally, we evaluate the value of redundancy for the purpose of remote sensor validation in decentralized wastewater treatment systems.

9 *Keywords:* data quality, drift, fault detection and identification,  
10 ion-selective electrodes, predictive maintenance, wastewater

---

## 11 **1. Introduction**

12 By several accounts, the lack of online sensor data quality poses a long-  
13 standing challenge for both the advancement of environmental science and  
14 engineering practice (Rieger et al., 2005, 2006; Rosén et al., 2008; Rieger  
15 et al., 2010; Haimi et al., 2013; Corominas et al., 2018). It is therefore not  
16 surprising that considerable time and energy has been invested in methods  
17 for automated quality assessment and quality control of online measurement  
18 devices (e.g., Thomann et al., 2002; Thomann, 2008; Corominas et al., 2011;  
19 Spindler and Vanrolleghem, 2012; Alferes et al., 2013; Spindler, 2014; Villez  
20 and Habermacher, 2016; Le et al., 2018).

21 Methods that are finding their way into practice today mainly consist of  
22 sanity checks. In the authors’ experience, these work rather well to detect  
23 and classify a subset of commonly recognized fault symptoms, including out-  
24 liers, spikes, stuck, and out-of-range values. For sensor faults that lead to  
25 more subtle symptoms, current practice relies primarily on regular on-site  
26 sensor maintenance, e.g. once every one or two weeks, to counter such subtle  
27 faults. For unstaffed wastewater treatment plants, on-site maintenance may

28 be feasible economically only if this is limited to once per year. This practical  
29 constraint to the adoption of quality assessment and control practices forms  
30 the primary motivation for this study.

31 The literature suggests that data-analytical techniques can enable auto-  
32 mated and remote detection of sensor faults. Without exception, such tech-  
33 niques rely on redundant relationships and can therefore be categorized by  
34 the type of redundancy that is used. A first category consists of techniques re-  
35 lying on reference measurements and computing a deviation between online  
36 sensor signal and the reference signal. A second category relies on hard-  
37 ware redundancy by placing multiple online sensors, possibly built around  
38 a distinct measurement principle, in the same location and then computing  
39 deviations between them. A third category relies on temporal redundancy,  
40 essentially assuming that meaningful changes in the sensor signal can only be  
41 smooth when measured with a sufficiently high frequency. Finally, the fourth  
42 category relies on spatial redundancy, relating signals produced at distinct  
43 locations or for different measured variables. Examples of this last cate-  
44 gory include both methods based on first principles, e.g. balance equations,  
45 as well as methods rooted in statistical practice, e.g. principal component  
46 analysis. Importantly, each of these advanced methods require tuning to  
47 maximize the number of true alarms and to ensure suitable quality control  
48 efforts while simultaneously minimizing the number of false alarms and fu-  
49 tile maintenance actions. Invariably, such tuning is obtained by means of  
50 a historical, fault-free data set from which acceptable limits for computed

51 residuals are derived. Consequently, this means that these methods rely on  
52 the availability of representative data of an acceptable quality. In addition,  
53 the use of most techniques implies that sensor fault symptoms can be as-  
54 sumed to appear independently from each other, i.e. the probability that  
55 two faults start at the same time is assumed to equal zero.

56 The prevalence of faults in actuators, sensors, and processes as well as  
57 the complexity of the fault detection and identification (FDI) task, has led  
58 to a plethora of methods that exploit one or more of the types of redundancy  
59 discussed above. In fact, the wealth of literature as well as the number  
60 of reviews on this or related topics (Venkatasubramanian et al., 2003c,a,b;  
61 Haimi et al., 2013; Corominas et al., 2018) suggest that the science and  
62 practice of FDI is all but settled, an observation also supported by no free  
63 lunch theorems (Wolpert, 1996).

64 Despite the tremendous amount of research on FDI methods, little is ac-  
65 tually known about the cause-and-effect relationships between sensor ageing,  
66 the occurrence of sensor faults and failures, and the production of faulty data.  
67 This is explained by the fact that the availability of information describing  
68 the exact circumstances under which faults occur or faulty data is produced,  
69 i.e. meta-data, is usually severely limited. This is the secondary motivation  
70 of this study.

71 To facilitate performance evaluation of FDI tools, the formulation of sim-  
72 ulation benchmarks has been an accepted practice in engineering sciences  
73 (Barty et al., 2006; Downs and Vogel, 1993). Similarly, the Benchmark Sim-

74 ulation Model No. 1 was conceived as a way to test and compare innovative  
75 FDI and control strategies (Jeppsson et al., 2007). Today, it is primarily used  
76 as a starting point for a family of plant-wide models of water resource recov-  
77 ery facilities (Nopens et al., 2009; Volcke et al., 2006). Actual benchmarking  
78 of FDI methods has been limited to one study so far (Corominas et al., 2011).  
79 The BSM family includes a set of sensor models which include sensor faults  
80 and this allows the user to add realism to the sensor signals. The simulated  
81 sensor faults always start at a time that is substantially later than the start  
82 of the simulated time. This provides ideal conditions for FDI method tuning  
83 as high-quality sensor data are always present in the first sections of the sim-  
84 ulated data set. Moreover, a simulated fault always appears independently  
85 of any other sensor fault, i.e. no two sensor faults are simulated to start at  
86 the same time or with the same direction or magnitude. We expect that the  
87 situation in real-world conditions is very different. We thus hypothesize that  
88 typical fault symptoms will appear at the same time and with similar direc-  
89 tions and magnitudes when exposed to the same harsh medium, especially  
90 when the same measurement principle is applied. Evaluating the merit of  
91 this hypothesis is the tertiary motivation of this study.

92 The following paragraphs are focused on the results and conclusions  
93 drawn directly from experimental data obtained during a long-term sensor  
94 exposure experiment. Additional insight is however obtained by studying a  
95 variety of dynamic models to describe our measurements.

## 96 2. Materials & Methods

### 97 2.1. Theoretical and real-world behavior of the ion-selective electrodes for pH 98 measurement

99 The ion-selective measurement principle for pH measurement is under-  
100 stood rather well. According to the Nernst equation (Westcott, 2012) one  
101 measures an electric potential  $E$  (in mV), which is related to the activity of  
102 the protons,  $[H^+]$ , in the measured medium in steady state:

$$E = E^0 + \frac{RT}{F} \ln([H^+]) \quad (1)$$

103 where  $E^0$  is the reference potential,  $F$  is the Faraday constant ( $96485.33289 \text{ C mol}^{-1}$ ,  
104 Taylor et al., 2007),  $[H^+]$  is the proton activity in the reference cell,  $R$  is the  
105 molar gas constant ( $8.3144598 \text{ J mol}^{-1} \text{ K}^{-1}$ , Taylor et al., 2007), and  $T$  is  
106 the temperature measured in Kelvin. The pH is defined as  $-\log[H^+]$  (Buck  
107 et al., 2002) so that  $S(T)$  is the temperature-specific sensitivity, which can  
108 be computed as:

$$S(T) = \frac{RT}{F \log(e)} \quad (2)$$

109 Most typically, pH sensors are designed to deliver 0 mV at pH 7 so that  
110  $E^0$  is theoretically 0 mV. Similarly, the theoretical sensitivity at standard

111 ambient temperature and pressure (SATP) thus is  $S(298.15) = 59.1593$  mV  
112 per pH unit. Because the actual values of these parameters tend to deviate  
113 from their theoretical values, it is common to identify their values through  
114 a 2-point calibration procedure. At the engineering department at Eawag,  
115 the most common practice is to use buffered calibration media with pH 4.01  
116 and 7.00 for validation, followed by calibration when the absolute deviations  
117 between the produced pH measurements and the known pH values exceed a  
118 predetermined threshold. The data end user sets this threshold. Depending  
119 on the application, this ranges from 0.1 to 0.4 pH units. The theoretical  
120 potential at pH 4.01 and SATP is 177.0 mV.

## 121 2.2. Studied sensors

122 A total of 12 pH sensors are produced by Endress+Hauser (Reinach,  
123 Switzerland). These sensors consist of 5 sensor types (T1-T5) whose exact  
124 type cannot be revealed due to a confidentiality agreement. The first eight  
125 sensors consist of pairs of four commercially available sensor types (T1-T4)  
126 which are typically sold with a one-year warranty agreement. The first (sec-  
127 ond) sensor in each pair is designated with an  $a$  ( $b$ ), e.g. T1a, T1b. The last  
128 4 pH sensors are replicates of a recently developed sensor prototype (T5) and  
129 are referred to as T5a, T5b, T5c, and T5d.

130 The first three sensor pairs (T1-T3) have been in use throughout a long-  
131 term exposure experiment which lasted for 731 days (Oct. 4th, 2016 – Oct.  
132 4th, 2018). An overview of this experiment is given in Fig. 1. The 4th pair

133 (T4) has been in use during the first half year and was replaced with the  
134 5th pair (T5) on April 3rd, 2017 (day 182) as (i) the T4 sensors exhibit a  
135 long response time (not shown) and (ii) the opportunity arose to test the T5  
136 prototypes. The T5a sensor stopped producing a meaningful signal on June  
137 30th, 2017 (day 270) while T5b became faulty (details below) on August  
138 31st, 2017 (day 332). These sensors were replaced with another sensor of  
139 the same prototype (T5) on Oct. 2nd, 2017 (day 364). In this last pair, one  
140 sensor (T5d) failed within 1 day (day 365) while the other (T5c) has been  
141 fully functional until the end of the experiment.

### 142 2.3. Long-term exposure experiment

143 The sensors are exposed to the contents of a reactor used primarily to  
144 study advanced control strategies for nitrite accumulation prevention in a  
145 urine nitrification process (Thürlimann et al., Submitted). To this end, the  
146 nitrified urine is pumped through a closed tube made from PVC with a flow  
147 rate of 43 L/h. The design of this tube equipped with sensor-holding locks  
148 is shown in the *Supplementary Information (Section B)*.

149 The treated urine is from anthropogenic origin during the whole experi-  
150 mental period. The treated urine was collected from male lavatories in the  
151 Forum Chriesbach building at Eawag, with exception of the period from day  
152 April 30th, 2018 to June 21st, 2018 (day 574-625), when it was collected from  
153 female lavatories in the same building. From October 4th, 2017 to November  
154 24th, 2017 (day 366 to 417), the reactor was additionally fed with a nitrite



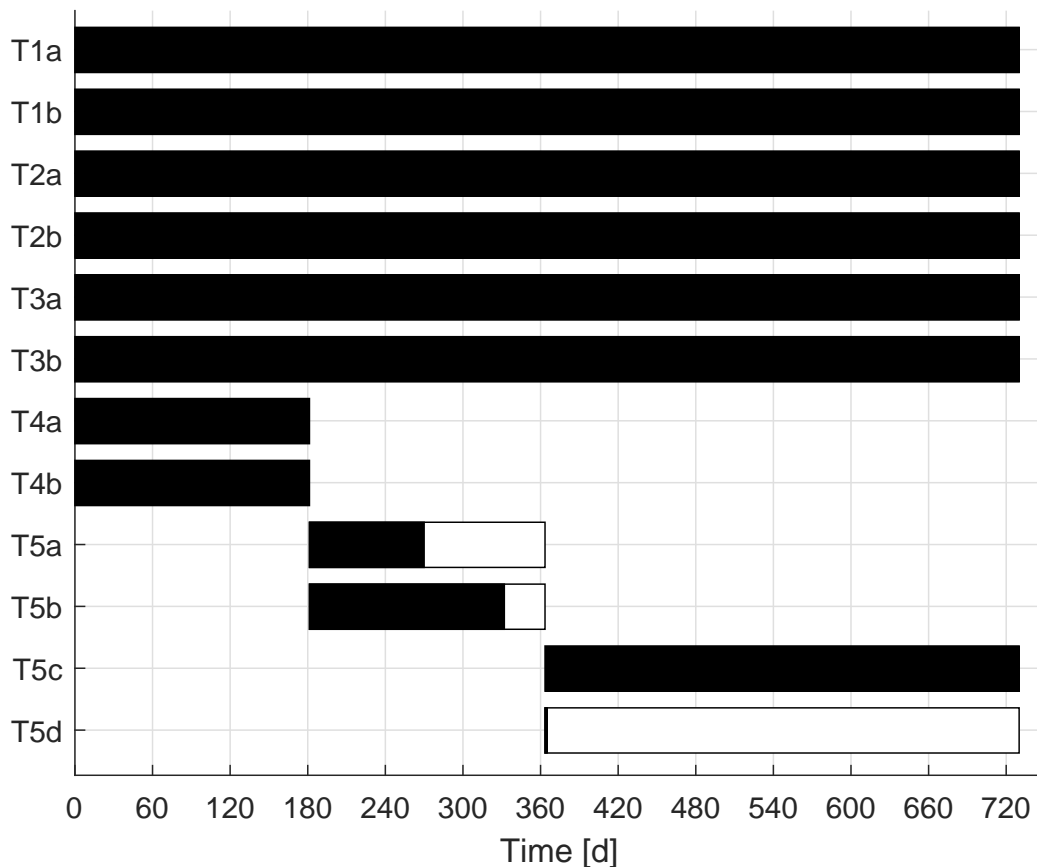


Figure 1: **Overview of the complete experimental campaign.** The periods of sensor exposure are indicated by rectangles. The periods during which the sensors produced meaningful data are marked black.

155 stock solution. During the experimental period, the measured concentra-  
 156 tions of nitrogen species in the nitrified urine ranged between 1180 and 2730  
 157 mgN/L (mg atomic nitrogen per liter) for total ammonia, 0 and 82 mgN/L  
 158 for nitrite, and 1290 and 2720 mgN/L for nitrate. These measurements are  
 159 copied from Thürlimann et al. (Submitted) and are shown in the *Supple-*  
 160 *mentary Information (Section C)*. The pH value of the nitrified urine, as

161 measured by two independent and regularly calibrated pH sensors installed  
162 directly in the reactor, ranged between 5.7 and 7.3.

#### 163 2.4. Sensor characterization tests

164 At regular intervals, the sensors were removed from their normal position  
165 and exposed to other media for sensor characterization. This was executed  
166 47 times in total. The exact times of these sensor characterization tests are  
167 listed in the *Supplementary Information (Section G.1)*. Two pairs of tests  
168 were executed on the same day to ensure acceptable experimental repro-  
169 ducibility (day 70: tests 11-12; day 351: tests 29-30). The selected media  
170 include (C4) pH 4.01 calibration solution (CPY20-C10A1, Endress+Hauser,  
171 Reinach, Switzerland); (C7) pH 7.00 calibration solution (CPY20-E10A1,  
172 Endress+Hauser, Reinach, Switzerland); (U4) nitrified urine at pH 4; (U7)  
173 nitrified urine at pH 7; and (W) tap water. For the present work, only the  
174 exposure to W, C4, and C7 is relevant. This occurs in five distinct phases  
175 (P0-P4), each lasting at least 5 minutes and exposing the sensors to W, C4,  
176 C7, C4, and W in this order. Exemplary results are shown in Fig. 2 and  
177 discussed in detail below.

178 Raw potential measurements recorded during P1, P2, and P3 are used  
179 to compute the offset ( $\tilde{E}^0$ ) and two measurements of the sensitivity ( $\tilde{S}_D$  and  
180  $\tilde{S}_R$ ). In line with (Carr, 1993), the following steps are applied for every sensor  
181 and every sensor characterization test:

- 182 1. Compute the median value among the potential measurements collected

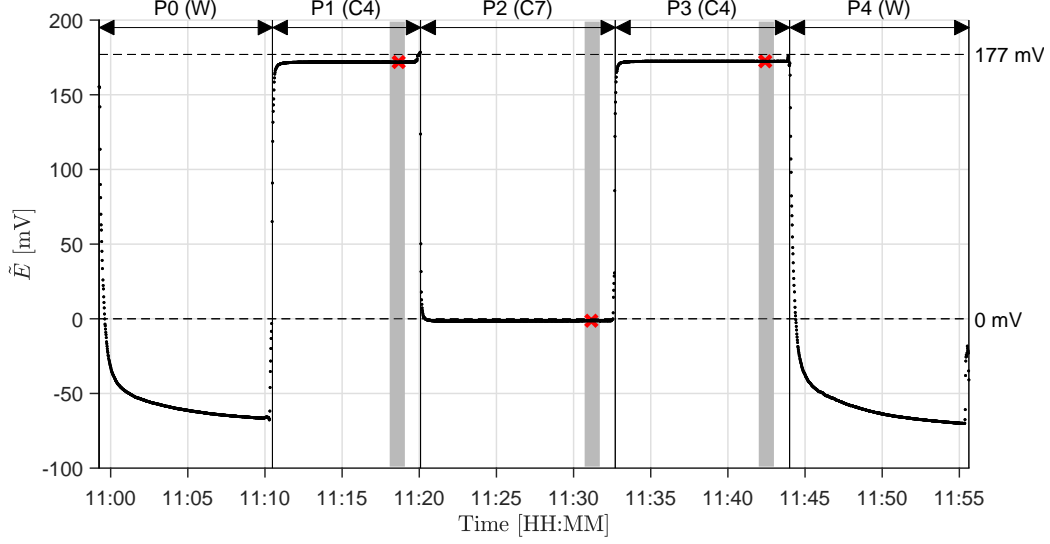


Figure 2: **Exemplary sensor characterization test.** Raw data obtained in the first sensor characterization test with sensor T1a. The measured potential decays during P0, P2, and P4, while it increases during P1 and P3. Steady state is reached quickly in P1, P2, and P3. The theoretical potential values for P1, P2, and P3 are indicated with dashed horizontal lines. Grey shading indicates the data used to obtain the potential measurements (2 to 1 minute before phase change). The selected median potential values are shown with red crosses.

- 183 in P1, P2, and P3 between 2 and 1 minutes before the start of the next  
184 phase (P2, P3, and P4). Refer to these values as  $E^{P1}$ ,  $E^{P2}$ , and  $E^{P3}$   
185 2. The sensor offset is defined as  $\tilde{E}^0 = \tilde{E}^{P2}$ .  
186 3. The decay potential sensitivity is defined as  $\tilde{S}_D = \frac{\tilde{E}^{P1} - \tilde{E}^{P2}}{7.00 - 4.01} = \frac{\tilde{E}^{P1} - \tilde{E}^{P2}}{2.99}$ .  
187 4. The decay potential sensitivity is defined as  $\tilde{S}_R = \frac{\tilde{E}^{P3} - \tilde{E}^{P2}}{7.00 - 4.01} = \frac{\tilde{E}^{P3} - \tilde{E}^{P2}}{2.99}$ .

188 These steps are demonstrated below with a practical example.

### 189 2.5. Drift model

190 The results shown below indicate that the offset significantly varies over  
191 time while the sensitivity remains remarkably stable in all studied sensors.

192 We describe the observed drift of the offset by means of two models.

### 193 2.5.1. Model 1 - Constant trend followed by linear trend

194 For the first model, we apply a modified version of the excessive drift  
 195 model proposed for the BSM family (Rosén et al., 2008). This model simu-  
 196 lates  $E^0(t)$ , the sensor offset, as:

$$E^0(t) = d_o + r_d H(t - t_f) \quad (3)$$

197 with  $d_o$  the initial offset,  $r_d$  the drift rate parameter,  $H(\cdot)$  the Heaviside  
 198 function ( $H(a) = 1$  if  $a \geq 0$ ,  $H(a) = 0$  otherwise),  $t$  the time since sensor  
 199 installation, and  $t_f$  the time of the drift onset. The applied modification con-  
 200 sists of adding the parameter  $d_o$ . To fit this model, the offset measurements,  
 201  $\tilde{E}^0(t_h)$ , collected at discrete time instants  $t_h$ , are assumed to exhibit inde-  
 202 pendently and identically distributed measurement errors,  $\epsilon_h$ , drawn from a  
 203 normal distribution with zero mean and standard deviation,  $\sigma_\epsilon$ :

$$\tilde{E}^0(t_h) = E^0(t_h) + \epsilon_h, \epsilon_h \sim N(0, \sigma_\epsilon) \quad (4)$$

204 Values for the 4 parameters  $d_o$ ,  $t_f$ ,  $r_d$ , and  $\sigma_\epsilon$  are obtained independently  
 205 for all sensors through maximum likelihood estimation (MLE). Once cali-  
 206 brated, the model is used to obtain the estimated mean and point-wise stan-

207 dard deviations for the sensor offset,  $\mu_1(t) = \mathbb{E}(E^0(t))$  and  $\sigma_1(t)$ , while using  
 208 the estimates of  $t_f$  and  $\sigma_\epsilon$  as fixed hyperparameter values.

### 209 2.5.2. Model 2 - Integrated Brownian motion for a single sensor

210 In model 2, we assume instead that the recorded offset measurements  
 211 are generated by an integrated Brownian motion. This is a continuous-time  
 212 stochastic process, which reflects that the drift rate is subject to unmeasured  
 213 disturbances:

$$\dot{r}_d(t) = \gamma(t)dt, r_d(0) = r_{d,o}, \gamma(t) \sim N(0, \sigma_\gamma), \quad (5)$$

$$\dot{E}^0(t) = r_d(t)dt, E(0) = d_o, \quad (6)$$

$$\tilde{E}^0(t_h) = E^0(t_h) + \epsilon_h, \epsilon_h \sim N(0, \sigma_\epsilon) \quad (7)$$

214 This model also includes 4 parameters: the initial drift rate ( $r_{d,o}$ ); the  
 215 initial offset ( $d_o$ ); an input noise standard deviation controlling the rate by  
 216 which the drift rate changes ( $\sigma$ ); and an output noise standard deviation  
 217 ( $\sigma_\epsilon$ ). As with model 1, parameter values are obtained through MLE. This is  
 218 achieved by formulating the above process as a Gaussian process (Rasmussen  
 219 and Williams, 2006). This also enables to compute expected values and  
 220 associated point-wise standard deviations,  $\mu_2(t) = \mathbb{E}(E^0(t))$  and  $\sigma_2(t)$ , with  
 221 the estimates of  $\sigma_\gamma$  and  $\sigma_\epsilon$  now used as fixed hyperparameter values.

222 *2.5.3. Model 3 - Integrated Brownian motion for multiple sensors*

223 A third model is derived from Eqs. 5-7 by considering that two sensors  
224 of the same type may be characterized by distinct initial conditions ( $r_{d,o}$ ,  
225  $d_o$ ) but the same noise parameters ( $\sigma_\epsilon$ ,  $\sigma_\gamma$ ). This lead to a model with six  
226 parameters ( $d_o^a$ ,  $d_o^b$ ,  $r_{d,o}^a$ ,  $r_{d,o}^b$ ,  $\sigma_\epsilon$ ,  $\sigma_\gamma$ ), instead of two models with 4 parameters  
227 each. Their values are again obtained via MLE and used to obtain calibrated  
228 predictions ( $\mu_3(t) = \mathbb{E}(E^0(t))$ ,  $\sigma_3(t)$ ), once again using the estimates of  $\sigma_\gamma$   
229 and  $\sigma_\epsilon$  as fixed hyperparameter values.

230 *2.5.4. Model evaluation*

231 The proposed models are evaluated through visual inspection of the mea-  
232 surements, predictions, and residuals between the measurements and predic-  
233 tions. In the present case, such a visual inspection is considered sufficient to  
234 select a suitable model.

235 *2.5.5. Implementation*

236 All data collected during the sensor characterization tests and all code  
237 necessary to reproduce our results is added in the *Supplementary Information*  
238 (*Section A*).

239 **3. Results**

240 *3.1. Sensor characterization tests: Example*

241 Fig. 2 shows the data obtained in the first sensor characterization test  
242 with sensor T1a on Oct. 6th, 2016 (day 3). The raw potential measurement

243 decreases during P0, increases to a steady value in P1, decreases to a steady  
 244 value in P2, increases to a steady value in P3, and decreases again in P4.  
 245 The time intervals used for computation of  $\tilde{E}^{P1}$ ,  $\tilde{E}^0$ , and  $\tilde{E}^{P3}$  (in calibration  
 246 medium, pH = 4, 7, and 4) are indicated by grey shading. One can see  
 247 that the measured offset  $\tilde{E}^0$  is slightly below 0 mV (−1.30 mV). The values  
 248 for  $\tilde{E}^{P1}$  and  $\tilde{E}^{P3}$  are slightly lower than their ideal value (171.9 and 172.4  
 249 mV). The measured rise and decay sensitivities are therefore  $\tilde{S}_D = 57.73$  and  
 250  $\tilde{S}_R = 57.90$  mV per pH unit. The results of every sensor characterization  
 251 test are visualized in the *Supplementary Information (Section G.2)*.

### 252 3.2. Long-term trends in the offset measurements within the warranty period

253 Fig. 3 displays the measured offsets in all sensors throughout the exper-  
 254 imental period. The recorded values collected within the warranty period  
 255 (1 year) range from approximately 0 mV (no offset) to roughly −70 mV.  
 256 All commercially available sensors (T1-T4) produce a decaying trend in the  
 257 offsets. The firstly recorded offsets for the T1-T3 sensors are small in magni-  
 258 tude and concentrate around 0 mV. In contrast, the T4 sensors offset values  
 259 indicate a shock effect producing a shift of −20 and −45 mV (T4a, T4b)  
 260 within days from installation. This is explained by the manufacturer as an  
 261 effect of the high ammonium concentration in the medium and should only  
 262 be expected for this specific type of sensors. The accumulated drift in the  
 263 T1 sensors is at most −25 mV after one year while the T2 and T3 sensors  
 264 exhibit an offset of −75 mV after one year. Without calibration, this means

265 the T1 sensors can produce a pH value as high as 7.4 when the true pH is 7.  
 266 The T2 and T3 sensors will produce a pH value as high as 8.3 in the same  
 267 circumstances. Due to failure of T5d, no offsets could be measured for this  
 268 sensor. The remaining prototypes (T5a/b/c) do not produce a significant  
 269 offset at any time, except for T5b which produces a dramatic shift in the  
 270 offset during three sensor characterization tests executed prior to replace-  
 271 ment. A detailed inspection of the T5b measurements revealed that the first  
 272 symptoms of sensor degradation can be observed on August 31st, 2017 (day  
 273 332). This is however only obvious when comparing these measurements  
 274 with the simultaneous T1b/T2b/T3b measurements (see the *Supplementary*  
 275 *Information, Section D*). In all cases, except for the T4 and T5a/b pairs, the  
 276 difference between offsets in sensors of the same type remains rather small  
 277 with 1 year of installation, with a maximal difference of 16.7 mV recorded  
 278 with the T2 sensors. Taking the 0.1 pH threshold discussed above as a  
 279 guideline, one could propose to validate and calibrate the sensors when their  
 280 potential measurements are 5.9 mV apart. This happens for the first time  
 281 for the T1, T2, and T3 sensors on day 127, 79, and 309. By these times,  
 282 the absolute offsets are already larger than this accepted threshold so that  
 283 the relative difference between sensors of the same type is unlikely a good  
 284 measure to trigger sensor maintenance.

285 Fig. 4 shows offsets for the sensors T1a, T3a, and T3b collected in the first  
 286 year of the experiment as a function of the difference in the offset between  
 287 T1a and T3a (left panel) and T3b and T3a (right panel). The left panel



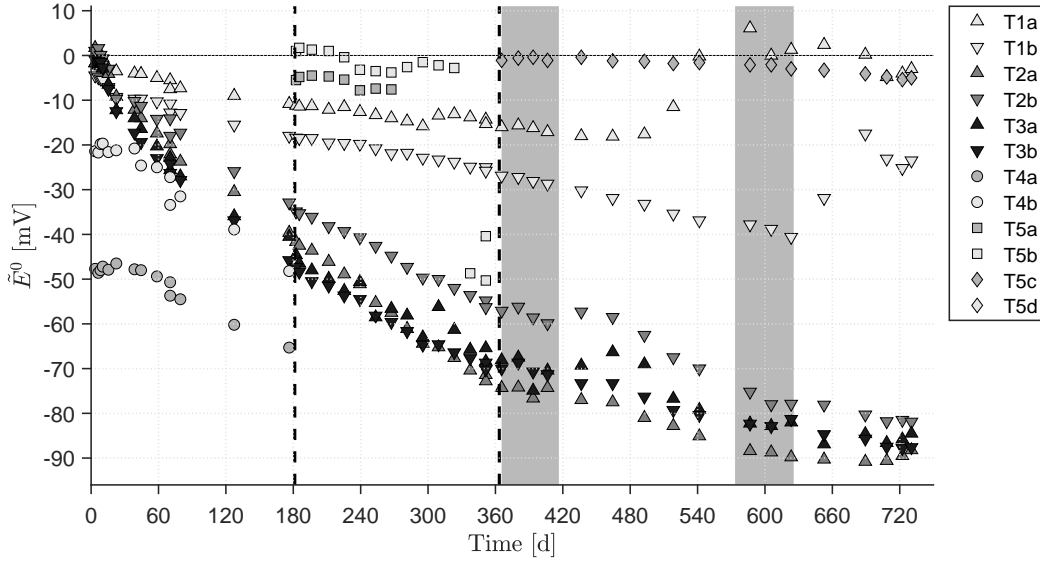


Figure 3: **Offset in all studied sensors as a function of time.** Vertical lines indicate a change of installed sensors (see Fig. 1). Grey bands indicate a change of reactor medium (see Section 2.3). The commercially available sensors (T1-T4) exhibit drift from the start of installation while the prototypes (T5) exhibit close to no drift when otherwise functioning properly. A significant shock effect is observed for the T4 sensors at the start of the experiment but not for any other sensor.

288 suggests that offset difference between sensors can be predictive of the offset  
 289 in an individual sensor. The right panel shows that this is less likely to be  
 290 successful for sensors of the same sensor type, as also described above. This  
 291 is considered an important opportunity for further research, which we discuss  
 292 further below.

### 293 3.3. Long-term trends in the offset measurements beyond the warranty period

294 The offset measurements obtained after the warranty period expired ex-  
 295 hibit two phenomena that are surprising (Fig. 3). The first phenomenon is  
 296 the rise of the offset of the T1a sensor after 480 days of exposure and a similar

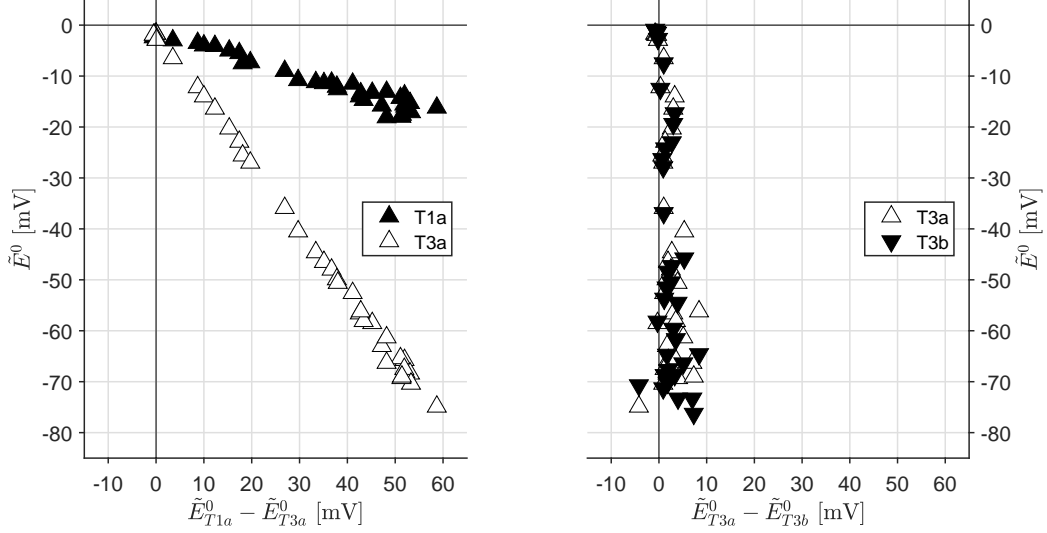


Figure 4: **Offset measurements as a function of relative deviations in the offset measurements.** *Left panel:* Offsets of sensor T1a and T3a as a function of the difference of these offsets. These data are suggestive of a close to linear relationship between sensor offsets and the offset difference. *Right panel:* Offsets of sensors T3a and T3b relative to the difference of these offsets. The difference in offset remains small and there is no obvious relationship in this case.

297 rise of the offset of the T1b sensor after 630 days of exposure. Considering  
 298 that this appears at distinct times in the lifetime of the T1 sensors, this can-  
 299 not be explained as a direct effect of medium composition changes. Based on  
 300 information provided by the sensor manufacturer, this type of drift rate sign  
 301 reversal is unique for the T1 sensors and is unlikely to be observed with any  
 302 other sensor type covered in this study. It is the opinion of the authors that  
 303 the time for this reversal is difficult to predict in advance. For this reason,  
 304 this phenomenon is best handled as an unmeasured process disturbance.

305 The second phenomenon consists of the rather flat to increasing profile of  
 306 the offset measurements in the T2 and T3 sensors between day 360 and day

480. Before and after this period, the drift rate in these sensors are visually similar. Given the synchronicity of this effect between 4 pH sensors, it is hypothesized that this change in the drift rate is influenced by the deliberate addition of nitrite in the form of  $\text{NaNO}_2$  salt to the reactor contents from day 366 to 417. The nitrite addition affected the biomass concentration and the concentrations of all dominant nitrogen species (ammonia, nitrite, nitrate, see *Supplementary Information, Section C*) and may also have affected the ion strength and conductivity of the reactor contents. Due to this combination of effects, the available data only offers an incomplete understanding of the complete chain of causes and effects between the nitrite addition and the observed changes in the sensor drift rates. For this reason, the effects of changing media composition on the sensor drift rate is best also considered an unmeasured process disturbance.

### 3.4. Long-term trends in the sensitivity measurements

Fig. 5 displays the computed sensitivity measurements for the potential rise ( $\tilde{S}_R$ ) during the complete experimental period. These measurements do not exhibit strong trends in any particular direction. The sensitivity measurements fall between 54.9 and 62.1 mV per pH unit. This means that one can expect to measure a pH value between 5.95 and 6.08 when (i) the true pH value is 6 and (ii) any offset is corrected for. The same graph also shows the theoretical value of the sensitivity according to (2) and the recorded temperature. This profile is very similar to the recorded sensitivity profiles

and explains most of the variations in the sensitivity measurements, which are small anyway. The same conclusions are drawn from the computed sensitivity measurements for the potential decay ( $\tilde{S}_D$ , see *Supplementary Information, Section E*).

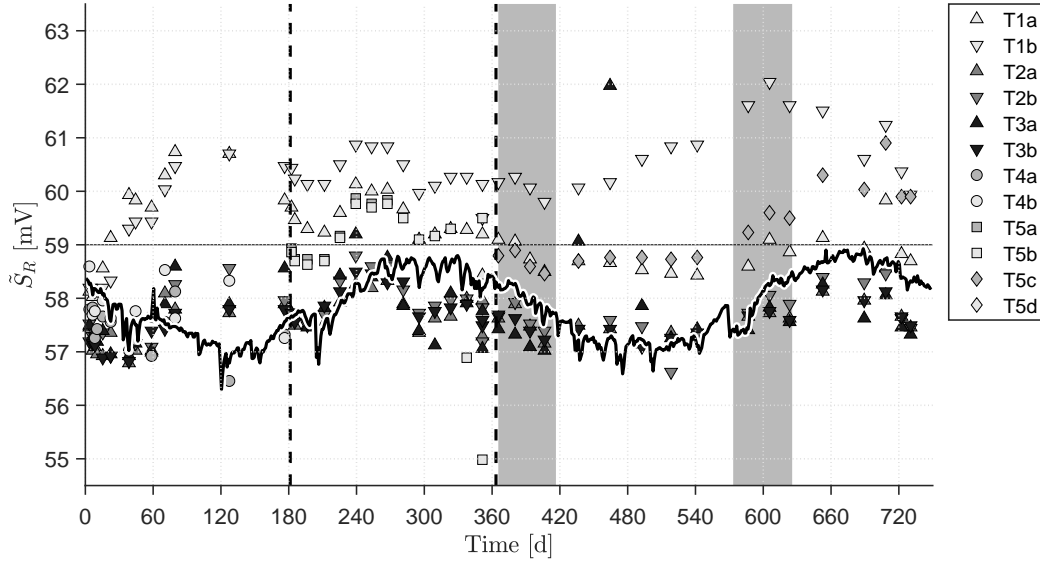


Figure 5: **Sensitivity measurements for the potential rise as a function of time.** Vertical lines indicate a change of installed sensors (see Fig. 1). Grey bands indicate a change of reactor medium (see Section 2.3). A black line shows the theoretically expected sensitivity computed with (2). Variations in the sensitivity are small and follow the theoretical sensitivity closely.

### 3.5. Drift models

For practical intents and purposes, the sensitivity – when corrected for temperature variations – can be considered constant for the considered process and sensors. We therefore focus on further analysis of the offset measurements.

338 The left panel of Fig. 6 shows the offset measurements for the T2a and  
 339 T2b sensor together with the model predictions and their confidence bounds.  
 340 The right panel of Fig. 6 shows the prediction residuals. With Model 1,  
 341 the time of the drift onset ( $t_f$ ) is always identified as a time before the first  
 342 measurement was obtained (2.1 and 2.3 days), suggesting that drift occurs  
 343 throughout the experiment. The same kind of result is obtained with every  
 344 other commercially available sensor type (T1-T4), except for the T1a sensor  
 345 (see the *Supplementary Information (Section F)*). More importantly however  
 346 is that Model 1 offers a rather poor description of the data. The confidence  
 347 intervals are wide and the residuals are clearly auto-correlated. In contrast,  
 348 Models 2 and 3 provide narrower confidence intervals and residuals that do  
 349 not suggest presence of autocorrelation. There are no clear differences in  
 350 performance between these two models so that Model 3, which has fewer free  
 351 parameters, is preferred. The modeling results for the T1 and T3 sensors lead  
 352 to the same conclusions. For these results and all parameter estimates, we  
 353 refer to the *Supplementary Information (Section F)*. For the T4 sensors, all  
 354 model types delivered the same, adequate performance. This may indicate  
 355 that (a) the T4 sensors exhibit a drift which is influenced less by unmeasured  
 356 disturbances and therefore occurs with a close to constant rate or (b) that  
 357 the shortened exposure – 6 months in this case – was too short to capture  
 358 the long-term effects of unmeasured disturbances.

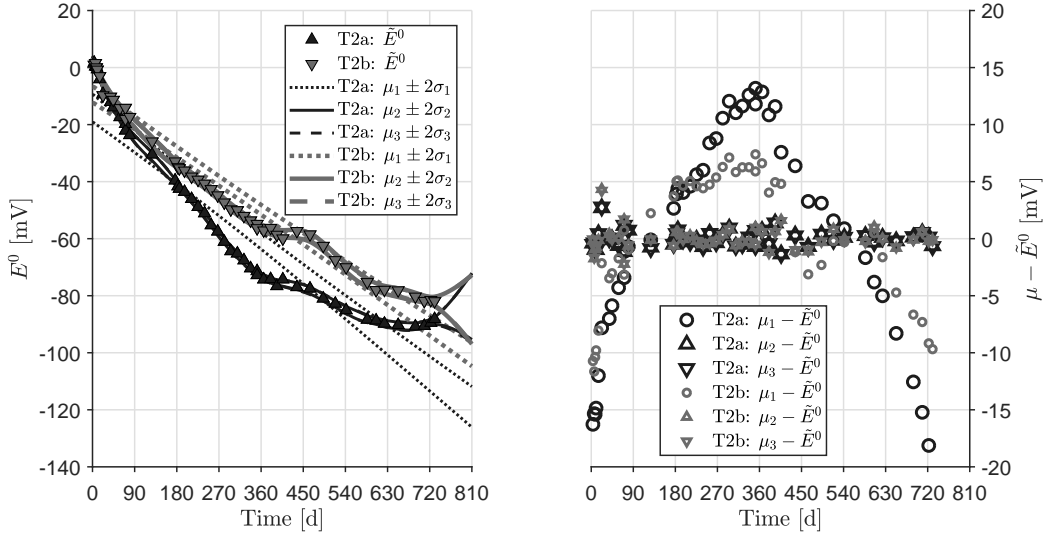


Figure 6: **Modeling results for the T2 sensors.** *Left panel:* Offset confidence bounds ( $\mu \pm 2\sigma$ ) obtained with models 1 ( $\mu_1, \sigma_1$ ), 2 ( $\mu_2, \sigma_2$ ), and 3 ( $\mu_3, \sigma_3$ ). *Right panel:* Residuals between expected values ( $\mu$ ) and measured potentials ( $\tilde{E}^0$ ). Model 1 does not describe the data well, leading to larger confidence bounds and auto-correlated residuals. Models 2 and 3 fit the data well and their predictions are hard to distinguish from each other.

#### 359 4. Discussion

360 This study present the first peer-reviewed results with which the effect  
 361 of long-term wear-and-tear on water quality sensors deployed in wastewater  
 362 treatment plants is assessed and evaluated in a systematic manner and at  
 363 this scale (12 sensors). The experimental results reveal that commonly held  
 364 assumptions regarding the occurrence of sensors faults and fault symptoms  
 365 are false. First, it is demonstrated that drift in pH sensors occurs simul-  
 366 taneously in all commercially available sensors. Second, it is demonstrated  
 367 that drift occurs as soon as a sensor is deployed in the measured medium.  
 368 In some cases, the immediate onset of drift is paired by a significant shift in

the offset. Importantly, the data needed to compute the offsets and sensitivities as a function of time are also available in modern pH instruments in the form of a calibration logbook that can be accessed through standardized communication protocols (e.g., Modbus).

These observations have important consequences for the development of methods for fault detection and identification (FDI). Indeed, *(i)* one cannot assume that faults appear independently in distinct sensors and *(ii)* one cannot assume to have access to a fault-free historical data set. Naturally, this also holds in the context of simulation-based benchmarking of FDI methods. Consequently, it is our opinion that the development of FDI methods and model-based benchmarking should be focused on methods that do not rely on such assumptions.

Fortunately, our results also reveal a number of opportunities for the use and maintenance of ion-selective measurements. First, the prototype sensors tested in this study exhibit a remarkably stable offset. While these sensors appear prone to failure, as one might expect from a prototype, this suggests that practically drift-free yet economical pH sensors will enter the market soon. Second, the recorded sensitivity measurements in all sensors hover around the ideal values and are remarkably stable throughout the experimental period. Such a stable sensitivity lends support for advanced monitoring and control strategies which are inherently robust to changes in the offset but still assume a rather stable sensitivity (Villez and Habermacher, 2016; Thürlimann et al., 2018a,b). Third, it was shown that the offset difference

between two pH sensors in the same medium can be predictive of the offset of the individual pH sensors, however only if two sufficiently distinct sensor types are selected. Combined with a stable sensitivity, this means that the deviation between two online pH sensor signals could be used as a proxy for the deviation in each individual sensor. Such a proxy measurement could be very useful for remote sensor quality assessment and predictive sensor maintenance, especially since one can compute such deviations between on-line sensor signals while the sensors remain in their normal measurement location in the monitored reactor.

The obtained offset measurements were studied in more detail by comparing the fit of 3 models. From this, it is concluded that the excessive drift model included in the BSM family (Rosén et al., 2008; Gernaey et al., 2014) cannot adequately describe the naturally occurring drift in ion-selective electrodes. Instead, the proposed stochastic model, specifically an integrated Brownian process, delivers a good description of the obtained data sets. In the authors' opinion, such a model should be included in the BSM family for realistic simulation of measurements obtained through ion-selective measurement principles. The obtained model also enables prediction of the expected offset measurement and associated confidence intervals beyond the last measurement. This means that such a model can be used for predictive sensor maintenance, e.g., by planning a new sensor validation and/or calibration before the predicted confidence interval exceeds a predetermined tolerance, each time also updating the parameters of the stochastic model. For this,



415 confidence intervals for the reference potential ( $E^0$ ) rather than for the mea-  
416 surements ( $\tilde{E}^0$ ) are expected to be most useful. Exploring the utility of this  
417 idea is considered for future research.

## 418 5. Conclusions

419 Despite the abundance of literature of fault detection and identification  
420 (FDI) methods, little is actually known about the cause-and-effect relation-  
421 ships between the exposure of water quality sensors to harsh conditions, such  
422 as wastewater media, and the occurrence of sensor faults and failures. This  
423 first long-term study of the ageing of 12 individual pH sensors gives valuable  
424 insight into this challenge. First, it is concluded that commonly held assump-  
425 tions in FDI method development and evaluation, such as the availability of  
426 fault-free historical data and independent onsets of sensor faults, are invalid  
427 for pH sensors based on the ion-selective measurement principle. In addition,  
428 the effects of offset drift in redundant sensors is unlikely to be identified early  
429 if these sensors are of the exact same type and exposed to the same medium.  
430 A stochastic model is shown to offer a good description of the observed drifts  
431 of the sensor offsets and perform better than a previously established drift  
432 model. Finally, our results suggest that newly developed pH sensors which  
433 exhibit stable offsets will enter the commercial market soon.

## 434 6. Acknowledgements

435 This research was made possible by the Swiss National Foundation (Project:  
436 157097). Mr. Ohmura’s contributions are financially supported by Toshiba,  
437 Tokyo, Japan. Dr. Carbajal’s contributions are financially supported by  
438 Eawag Discretionary Funds (grant no.: 5221.00492.011.05, project: DF2017/EMUmore).  
439 All sensors were provided at no cost by Endress+Hauser. We thank Daniel  
440 Iten and Stefan Vogel from Endress+Hauser for their valuable advice and  
441 input to this study. The stochastic models were calibrated with the GPML  
442 toolbox v4.2 (Rasmussen and Nickisch, 2005).

## 443 References

- 444 Alferes, J., Tik, S., Copp, J., Vanrolleghem, P. A., 2013. Advanced monitor-  
445 ing of water systems using in situ measurement stations: data validation  
446 and fault detection. *Water Science and Technology* 68 (5), 1022–1030.
- 447 Barty, M., Patton, R., Syfert, M., de las Heras, S., Quevedo, J., 2006. In-  
448 troduction to the DAMADICS actuator FDI benchmark study. *Control*  
449 *Engineering Practice* 14 (6), 577–596.
- 450 Buck, R., Rondinini, S., Covington, A., Baucke, F., Brett, C., Camoes, M.,  
451 Milton, M., Mussini, T., Naumann, R., Pratt, K., Spitzer, P., 2002. Mea-  
452 surement of pH. definition, standards, and procedures (iupac recommen-  
453 dations 2002). *Pure and Applied Chemistry* 74 (11), 2169–2200.
- 454 Carr, J. J., 1993. *Sensors and circuits*. PTR Prentice Hall.

455 Corominas, L., Garrido-Baserba, M., Villegz, K., Olsson, G., Cortes, U.,  
 456 Poch, M., 2018. Transforming data into knowledge for improved wastew-  
 457 ater treatment operation: A critical review of techniques. *Environmental*  
 458 *Modelling and Software* 106, 89–103.

459 Corominas, L., Villegz, K., Aguado, D., Rieger, L., Rosén, C., Vanrolleghem,  
 460 P. A., 2011. Performance evaluation of fault detection methods for wastew-  
 461 ater treatment processes. *Biotechnology and Bioengineering* 108 (2), 333–  
 462 344.

463 Downs, J. J., Vogel, E. F., 1993. A plant-wide industrial process control  
 464 problem. *Computers and Chemical Engineering* 17 (3), 245–255.

465 Gernaey, K. V., Jeppsson, U., Vanrolleghem, P. A., Copp, J. B., 2014. Bench-  
 466 marking of control strategies for wastewater treatment plants. *Scientific*  
 467 *and Technical Report No. 23*. IWA Publishing.

468 Haimi, H., Mulas, M., Corona, F., Vahala, R., 2013. Data-derived soft-sensors  
 469 for biological wastewater treatment plants: An overview. *Environmental*  
 470 *Modelling and Software* 47, 88–107.

471 Jeppsson, U., Pons, M. N., Nopens, I., Alex, J., Copp, J. B., Gernaey, K. V.,  
 472 Rosén, C., Steyer, J., Vanrolleghem, P. A., 2007. Benchmark Simulation  
 473 Model No. 2: General protocol and exploratory case studies. *Water Science*  
 474 *and Technology* 56(8) (67-78).

475 Le, Q. H., Verheijen, P. J., van Loosdrecht, M. C., Volcke, E. I., 2018. Exper-  
 476 imental design for evaluating WWTP data by linear mass balances. Water  
 477 Research 142, 415–425.

478 Nopens, I., Batstone, D. J., Copp, J. B., Jeppsson, U., Volcke, E., Alex, J.,  
 479 Vanrolleghem, P. A., 2009. An ASM/ADM model interface for dynamic  
 480 plant-wide simulation. Water Research 7, 1913–1923.

481 Rasmussen, C. E., Nickisch, H., 2005. Gaussian processes for machine learn-  
 482 ing (GPML) toolbox.  
 483 URL <https://gitlab.com/hnickisch/gpml-matlab/>

484 Rasmussen, C. E., Williams, C. K., 2006. Gaussian processes for machine  
 485 learning. MIT press.

486 Rieger, L., Langergraber, G., Siegrist, H., 2006. Uncertainties of spectral in  
 487 situ measurements in wastewater using different calibration approaches.  
 488 Wat. Sci. Technol. 53(12), 187–197.

489 Rieger, L., Takács, I., Villez, K., Siegrist, H., Lessard, P., Vanrolleghem,  
 490 P. A., Comeau, Y., 2010. Data reconciliation for wastewater treatment  
 491 plant simulation studies – planning for high-quality data and typical  
 492 sources of errors. Water Environment Research 82, 426–433.

493 Rieger, L., Thomann, M., Gujer, W., Siegrist, H., 2005. Quantifying the  
 494 uncertainty of on-line sensors at WWTPs during field operation. Water  
 495 Research 39 (20), 5162–5174.

496 Rosén, C., Rieger, L., Jeppsson, U., Vanrolleghem, P. A., 2008. Adding re-  
 497 alism to simulated sensors and actuators. *Water Science and Technology*  
 498 57 (3), 337–344.

499 Spindler, A., 2014. Structural redundancy of data from wastewater treatment  
 500 systems. determination of individual balance equations. *Water Research*  
 501 57, 193–201.

502 Spindler, A., Vanrolleghem, P. A., 2012. Dynamic mass balancing for wastew-  
 503 ater treatment data quality control using CUSUM charts. *Water Science*  
 504 and *Technology* 65 (12), 2148–2153.

505 Taylor, B. N., Mohr, P. J., Douma, M., 2007. The NIST reference on con-  
 506 stants, units, and uncertainty.  
 507 URL `physics.nist.gov/cuu/index`

508 Thomann, M., 2008. Quality evaluation methods for wastewater treatment  
 509 plant data. *Wat. Sci. Technol.* 10, 1601–1609.

510 Thomann, M., Rieger, L., Frommhold, S., Siegrist, H., Gujer, W., 2002. An  
 511 efficient monitoring concept with control charts for on-line sensors. *Water*  
 512 *Science and Technology* 46 (4-5), 107–116.

513 Thürlimann, C. M., Dürrenmatt, D. J., Villez, K., 2018a. Soft-sensing with  
 514 qualitative trend analysis for control in full-scale wastewater treatment  
 515 plants. *Control Engineering Practice* 70, 121–133.

516 Thürlimann, C. M., Udert, K. M., Morgenroth, E., Villez, K., 2018b. Assess-  
 517 ment of two qualitative trend analysis tools for process control. In: 4th  
 518 IWA Specialized International Conference "Ecotechnologies for Wastewa-  
 519 ter Treatment" (EcoSTP2018), London, ON, Canada, June 25-27, 2018.

520 Thürlimann, C. M., Udert, K. M., Morgenroth, E., Villez, K., Submitted.  
 521 Handling sensor drift for stabilizing nitrite control during nitrification of  
 522 high strength wastewater by means of qualitative trend analysis.

523 Venkatasubramanian, V., Rengaswamy, R., Kavuri, S. N., 2003a. A review  
 524 of process fault detection and diagnosis – Part II: Qualitative models and  
 525 search strategies. *Computers & Chemical Engineering* 27 (3), 313–326.

526 Venkatasubramanian, V., Rengaswamy, R., Kavuri, S. N., Yin, K., 2003b. A  
 527 review of process fault detection and diagnosis – Part III: Process history  
 528 based methods. *Computers & Chemical Engineering* 27 (3), 327–346.

529 Venkatasubramanian, V., Rengaswamy, R., Yin, K., Kavuri, S. N., 2003c.  
 530 A review of process fault detection and diagnosis – Part I: Quantitative  
 531 model-based methods. *Computers & Chemical Engineering* 27 (3), 293–  
 532 311.

533 Villez, K., Habermacher, J., 2016. Shape anomaly detection for process mon-  
 534 itoring of a sequencing batch reactor. *Computers & Chemical Engineering*  
 535 91, 365–379.

- 536 Volcke, E. I., van Loosdrecht, M. C., Vanrolleghem, P. A., 2006. Continuity-  
537 based model interfacing for plant-wide simulation: A general approach.  
538 Water Research 15, 2817–2828.
- 539 Westcott, C., 2012. pH measurements. Elsevier.
- 540 Wolpert, D. H., 1996. The lack of a priori distinctions between learning al-  
541 gorithms. Neural Computation 8 (7), 1341–1390.